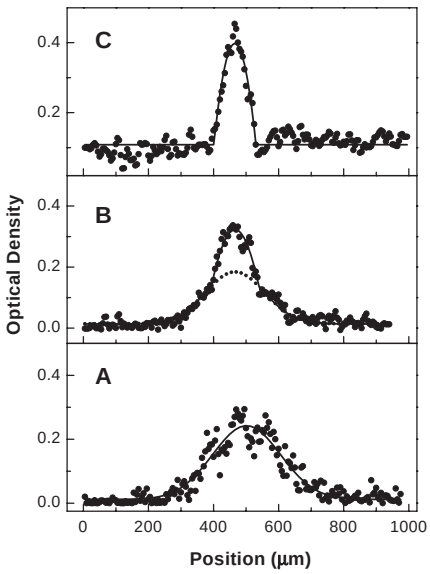

Fig. 4. Density profiles of three samples of ^{41}K after 15 ms of expansion, showing the transition to BEC. (**A**) Thermal sample at $T = 250$ nK. (**B**) Mixed sample at $T = 160$ nK. (**C**) Almost pure condensate. The lines are the best fit with a Gaussian for the thermal component and with an inverted parabola for the condensate component.

(*27*, *28*), which may represent a new system for quantum computing (*29*).

The possibility of sympathetic cooling to quantum degeneracy with a different species broadens the spectrum of coolable particles to include molecules as well (*30*). Because Rb is the workhorse for experiments on cold atoms, one could take advantage of recently demonstrated techniques for a simultaneous trapping of the partner species. For example, a BEC of ^{87}Rb has been produced in an optical dipole trap (*31*), which is an ideal tool to trap a large variety of atoms and molecules lacking a magnetic moment in their ground state. Sympathetic cooling in this kind of trap would have repercussions for high-resolution spectroscopy and metrology (*32*), tests of fundamental theories (*33*), and ultracold chemistry.

References and Notes

1. M. H. Anderson, J. R. Ensher, M. R. Mattews, C. E. Wieman, E. A. Cornell, *Science* **269**, 198 (1995).
2. K. B. Davis *et al*., *Phys. Rev. Lett.* **75**, 3969 (1995).
3. C. C. Bradley, C. A. Sackett, J. J. Tollet, R. G. Hulet, *Phys. Rev. Lett.* **75**, 1687 (1995).
4. M. Inguscio, S. Stringari, C. E. Wieman, Eds., *Bose-Einstein Condensation in Atomic Gases*, Proceedings of the International School of Physics "Enrico Fermi," Course CXL (IOS Press, Amsterdam, 1999).
5. D. G. Fried *et al.*, *Phys. Rev. Lett.* **81**, 3811 (1998).
6. A. Robert *et al*., *Science* **292**, 461 (2001); published online 22 March 2001 (10.1126/science.1060622).
7. S. L. Cornish *et al*., *Phys. Rev. Lett.* **85**, 1795 (2000).
8. M. Prevedelli *et al*., *Phys. Rev. A* **59**, 886 (1999).
9. D. J. Wineland, R. E. Drullinger, F. L. Walls, *Phys. Rev. Lett.* **40**, 1639 (1978).
10. C. J. Myatt *et al*., *Phys. Rev. Lett.* **78**, 586 (1997).
11. F. Schreck *et al*., *Phys. Rev. A* **87**, 011402(R)(2001).
12. G. Truscott, K. E. Strecker, W. I. McAlexander, G. B. Partridge, R. G. Hulet, *Science* **291**, 2570 (2001).
13. I. Bloch, M. Greiner, O. Mandel, T. W. Hänsch, T. Esslinger, *Phys. Rev. A* **64**, 021402(R) (2001).
14. F. S. Cataliotti *et al.*, *Phys. Rev. A* **57**, 1136 (1998).
15. B. De Marco, D. S. Jin, *Science* **285**, 1703 (1999).
16. F. Schreck *et al*., *Phys. Rev. Lett.* **87**, 080403 (2001).
17. This is a development of the scheme introduced in G. Ferrari, M.-O. Mewes, F. Schreck, C. Salomon, *Opt. Lett.* **24**, 151 (1999).
18. A near coincidence between the K ground-state and the Rb excited-state hyperfine splittings induces losses of Rb atoms from the MOTs, when K and Rb lights are injected simultaneously in the TA.
19. T. Esslinger, I. Bloch, T. W. Hänsch, *Phys. Rev.* A **58**, R2664 (1998).
20. A. Mosk *et al.*, preprint available at http://xxx.lanl.gov/abs/physics/0107075.
21. The interaction properties of ultracold atoms are described by a single parameter, namely the scattering length a, which we give in atomic units ($a_0 = 0.0529$ nm). The zero-energy collisional cross-section between distinguishable particles can be expressed as $\sigma = 4\pi a^2$. At finite energy, σ depends also on the sign of the scattering length. The mean-field interaction energy in a Bose-Einstein condensate can be expressed as $E = h^2na/(\pi M)$, where n is the gas density.
22. Because the evaporation ramp is optimized for K, at this stage the Rb sample typically contains less than 10^4 atoms and still follows a thermal distribution. Further reduction of the evaporation threshold results in a complete loss of all the Rb atoms.
23. F. Dalfovo, S. Giorgini, L. P. Pitaevskii, S. Stringari, *Rev. Mod. Phys.* **71**, 463 (1999).
24. G. Delannoy *et al*., *Phys. Rev. A* **63**, 051602(R) (2001).
25. C. Monroe, E. A. Cornell, C. A. Sackett, C. J. Myatt, C. E. Wieman, *Phys. Rev. Lett.* **70**, 414 (1993).
26. H. Wang *et al*., *Phys. Rev. A* **62**, 052704 (2000).
27. A. Fioretti *et al.*, *Phys. Rev. Lett.*, **80**, 4402 (1998).
28. S. J. J. M. F. Kokkelmans, H. M. J. Vissers, B. J. Verhaar, *Phys. Rev. A* **63**, 031601(R) (2001) and references therein.
29. D. DeMille, preprint available at http://xxx.lanl.gov/abs/quant-ph/0109083.
30. Trapped molecular samples at a few mK have recently been produced [H. L. Bethlem *et al.*, *Nature* **406**, 491 (2000)].
31. M. D. Barrett, J. A. Sauer, M. S. Chapman, *Phys. Rev. Lett.* **87**, 010404 (2001).
32. C. W. Oates, E. A. Curtis, L. Hollberg, *Opt. Lett.* **25**, 1603 (2000).
33. E. A. Hinds, K. Sangster, in *Time Reversal-The Arthur Rich Memorial Symposium*, M. Skalsey, P. H. Bucksbaum, R. S. Conti, D. W. Gidley, Eds. (American Institute of Physics, New York, 1993).

34. We benefited from stimulating discussions with all the colleagues of the laser cooling and BEC group at LENS. We thank W. Jastrzebski, N. Poli, F. Riboli, and L. Ricci for their contribution to the experiment; I. Bloch for useful hints for the construction of the magnetic trap; and R. Ballerini, M. DePas, M. Giuntini, A. Hajeb, and A. Orlando for technical assistance. Supported by the Ministero dell'Università e della Ricerca Scientifica; by the European Community under contract HPRICT1999-00111; and by the Istituto Nazionale per la Fisica della Materia, Progetto di Ricerca Avanzata "Photonmatter." G.R. is also at Dipartimento di Fisica, Università di Trento; R.B. is presently at the Department of Physics, University of Dayton, OH; A.S. is also at Dipartimento di Chimica, Università di Perugia; M.I. is also at Dipartimento di Fisica, Università di Firenze.

1 October 2001; accepted 11 October 2001
Published online 18 October 2001;
10.1126/science.1066687
Include this information when citing this paper.

Bulk-Like Features in the Photoemission Spectra of Hydrated Doubly Charged Anion Clusters

Xue-Bin Wang,[1,2] Xin Yang,[1,2] John B. Nicholas,[3] Lai-Sheng Wang[1,2]*

We produced gaseous hydrated clusters of sulfate and oxalate anions [$SO_4^{2-}(H_2O)_n$ and $C_2O_4^{2-}(H_2O)_n$, where $n = 4$ to 40]. Photoelectron spectra of these clusters revealed that the solute dianions were in the center of the water cluster, $(H_2O)_n$. For small clusters, these spectra were characteristic of the respective solutes, but beyond the first solvation shell ($n \approx 12$), features in the spectra from the solutes were diminished and a new feature from ionization of water emerged, analogous to bulk aqueous solutions. For large clusters with dimensions greater than 1 nanometer, the solute photoemission features disappeared and the spectra were dominated by the ionization of water as the solvent coverage increased. A smooth transition from gas-phase clusters to behavior of electrolyte solutions was clearly revealed, and the large solvated clusters can be used as molecular models to investigate the photophysics and chemistry of aqueous electrolyte solutions.

Cations often exhibit definitive solvation shells both in bulk aqueous solutions (*1, 2*) and in water clusters (*3*) because of their small sizes and strong solute-water interactions. However, the solvation of anions is more complicated, and microscopic information about their solvation is relatively limited despite their importance in chemistry and biochemistry (*4–6*). Most current research on solvated anion clusters has been devoted to the simple halide anions (*7–13*), with few studies on more complex anions (*14–16*).

Multiply charged anions are ubiquitous in aqueous solutions and biomolecules and constitute a vital class of complex anions (*17*). But there has been relatively little experimental and theoretical effort to elucidate their stability and solvation at a molecular level (*18–20*). Here, we report photoelectron spectra (PES) of large solvated clusters of two common inorganic doubly charged anions, $SO_4^{2-}(H_2O)_n$ and $C_2O_4^{2-}(H_2O)_n$ (n = 4 to 40), that provide a bridge between hydrated clusters and aqueous solutions and allow us to probe properties of aqueous electrolyte solutions in the gas phase. The analysis of the evolution of the PES with cluster size shows the dianions were solvated in the center of the water clusters. As the solvent number increased, PES features from the solutes diminished as a result of increased solvent coverage, and additional features from ionization of the solvent emerged. A gradual transition from molecular clusters to behavior of electrolyte solutions was clearly observed, and the solvated clusters may be viewed as molecular models for aqueous solutions.

The application of photoelectron spectroscopy to aqueous solutions has been extremely challenging because of the difficulties of handling solution samples under high-vacuum conditions (*21–23*). The use of hydrated ion samples provides an alternative approach (*7, 24, 25*), but it has not been possible to examine multiply charged anions until recently (*17, 26*). We used an electrospray ion source to produce the solvated clusters. The experimental apparatus, equipped with the electrospray source, an ion trap, and photoemission capability, has been described in detail (*27*). In the current study, a 10^{-4} M solution of Na_2SO_4 or $Na_2C_2O_4$ in a water-acetonitrile solution was used in the electrospray. Solvated clusters with a single doubly charged anion, $SO_4^{2-}(H_2O)_n$ or $C_2O_4^{2-}(H_2O)_n$, were readily produced for n = 4 to 60. A given solvated cluster of interest was selected and irradiated with a laser beam in the interaction zone of a magnetic-bottle photoelectron analyzer. Three detachment photon energies were used in the current experiment: 266 nm (4.661 eV), 193 nm (6.424 eV), and 157 nm (7.866 eV). Because the electron binding energies increase with cluster size, the highest photon energy at 157 nm was required to investigate the large clusters, whereas for smaller clusters PES at various photon energies were obtained.

Figure 1A shows the PES of $SO_4^{2-}(H_2O)_n$ from n = 4 to 40 at 157 nm. The electron binding energies were observed to increase monotonically with the solvent number. All of the features in the PES of the small $SO_4^{2-}(H_2O)_n$ clusters—including two well-separated bands at lower binding energies and a broad feature at higher binding energies—were due to electron emission from SO_4^{2-}, and they were similar to the PES of $Na^+(SO_4^{2-})$, as we showed in (*26*). The similarity among the spectra of the small clusters indicated that the SO_4^{2-} dianion remained intact in the solvated clusters. However, as the solvent number increased above $n \approx 12$, three gradual changes were observed in the PES. First, the relative intensity of the low binding energy feature from SO_4^{2-} seemed to decrease and almost disappeared in the large clusters. Second, a very intense peak emerged at the high binding energy side. Third, above $n \approx 12$, the gap between the first two bands became smaller, whereas it remained constant in the small clusters and in $Na^+(SO_4^{2-})$. The cutoff at the high binding energy side in each spectrum was due to the repulsive Coulomb barrier (RCB), which exists universally in multiply charged anions and essentially prohibits slow electrons (high electron binding energies) from being emitted (*17*).

The onset of the three spectral changes mentioned above was between n = 12 and 15 and became quite obvious beyond n = 16 (Fig. 1A). The solute features almost completely disappeared for $n > 30$. The high binding energy feature must be due to a new ionization channel that gained cross section with cluster size, whereas the detachment cross sections for the solute decreased with cluster size. The latter finding was confirmed when the experiment was performed at 193 nm, where only the first solute band could be observed for $n > 13$ because of the RCB that cut off the higher binding energy features. A significant reduction of electron count rates was observed at 193 nm for $n > 12$, consistent with the observation at 157 nm (Fig. 1A), and it became rather difficult for us to observe photoemission signals beyond n = 18, despite the photon energy still being above the RCB and the reasonable strength of the cluster mass signals.

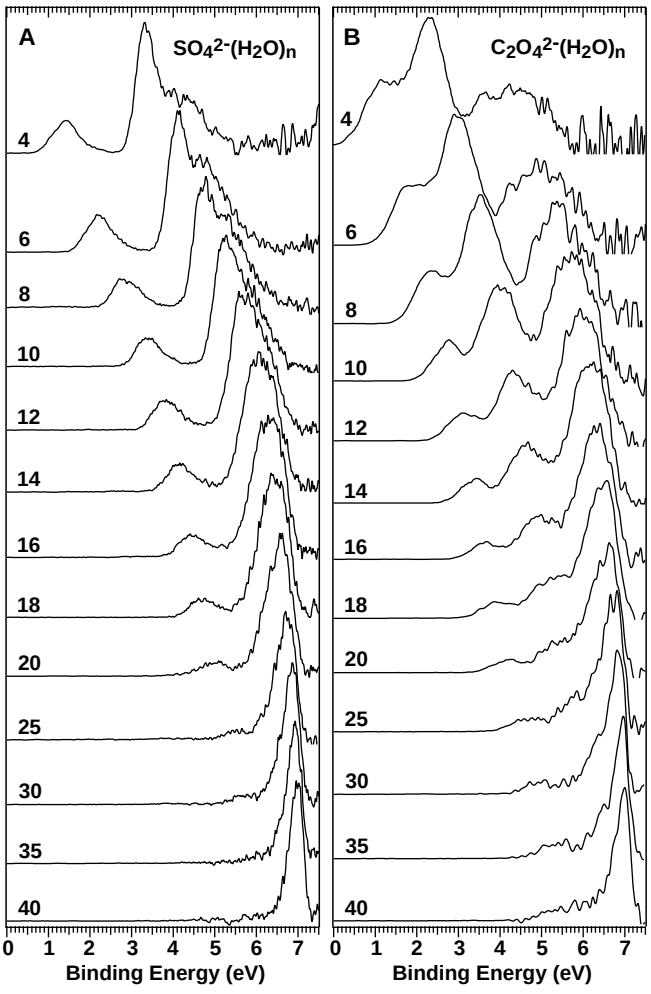

Fig. 1. Representative PES of (**A**) $SO_4^{2-}(H_2O)_n$ and (**B**) $C_2O_4^{2-}(H_2O)_n$ (n = 4 to 40) at 157 nm (7.866 eV). [All of the spectra for n = 4 to 40 for the sulfate clusters can be viewed at (*37*).]

[1]Department of Physics, Washington State University, 2710 University Drive, Richland, WA 99352, USA. [2]W. R. Wiley Environmental Molecular Sciences Laboratory, Pacific Northwest National Laboratory, Mail Stop K8-88, Post Office Box 999, Richland, WA 99352, USA. [3]Genentech Inc., 1 DNA Way, South San Francisco, CA 94080, USA.

*To whom correspondence should be addressed. E-mail: ls.wang@pnl.gov

Similar observations were made in the PES of $C_2O_4^{2-}(H_2O)_n$ (Fig. 1B). In smaller clusters (n = 4 to 10), PES features from the $C_2O_4^{2-}$ solute dominated. The three broad bands observed for n = 4 and 6 were similar to PES features observed for $Na^+(C_2O_4^{2-})$ (*28*). As the solvent number increased, the features from the solute gradually diminished, accompanied by the appearance of a strong feature at the high binding energy side. The PES spectral changes occurred in a cluster size range similar to that seen in $SO_4^{2-}(H_2O)_n$, except that the features from $C_2O_4^{2-}$ remained discernible even for $n > 30$, whereas in $SO_4^{2-}(H_2O)_n$ the solute features almost completely disappeared for $n > 30$. The new features that appeared in the large clusters in both solvated systems were nearly identical in spectral shape and binding energy.

The spectra presented in Fig. 1 represent transitions from the doubly charged solvated clusters to singly charged species. The spectral changes observed in the large solvated clusters were not anticipated, because as the solvent number increased the solutes were expected to remain intact. In particular, the loss of the solute PES features in the large clusters was a total surprise. Chemical changes, such as intracluster proton transfer, could be ruled out because the large solvated clusters represented more "diluted solutions," and the chemical equilibrium should favor the intact dianions as solvent number increased. In the only previous PES studies of large hydrated anions [i.e., $I^-(H_2O)_n$], PES features from the solute I^- were observed for n as large as 60 (*7*). Interestingly, the I^- anion has since been found to be on the surface of the water clusters (*8, 9*). The disappearance of the solute signals in the current systems suggested that the dianions might be solvated in the center of the water clusters, so that photoelectrons from the centrally located solute might not readily escape the increasing solvent layers. This difference between the dianions and I^- could arise from the stronger charge-dipole interactions between the dianions and water compared to the single diffuse charge of I^-. Our ab initio calculations for up to six water molecules showed that the water molecules indeed tend to solvate symmetrically around the dianions for both SO_4^{2-} (*26*) and $C_2O_4^{2-}$ (*28*).

This interpretation is supported by a previous photoelectron study at 21.2 eV of a highly concentrated aqueous solution of CsF (*22*). In this experiment, PES features from F^- were significantly reduced by a one-layer water solvation shell on F^- at the solution-vacuum interface (*29*). Furthermore, a small mixture of CsI into the CsF solution showed that PES features from I^- were actually enhanced because I^- displayed more surface activity (*22*). These observations in the bulk electrolyte solutions were consistent with the observations in the gas-phase solvated clusters, where I^- is known to be solvated on the outside of the water clusters (*8, 9*) and F^- is known to be solvated on the inside because of its strong charge-dipole interactions with water (*8, 9, 11*).

Our data on the solvated sulfate and oxalate dianions are consistent with those of the bulk electrolyte solutions. As the solvent number increased, the solutes were gradually being covered with water. The onset of the decreasing solute signals around n = 13 to 15 may suggest the completion of the first solvation shell. Although the number of water molecules in the first solvation shell for the dianions in bulk solutions was not definitively known (*2*), our observation was consistent with a previous molecular dynamics simulation that suggested that the first solvation shell for SO_4^{2-} consisted of about 13 water molecules (*20*). As more solvent molecules were added, the second solvation shell began to form, further reducing the solute PES signals. With about 30 water molecules, the signals from SO_4^{2-} were almost completely damped. The signals from $C_2O_4^{2-}$ were still visible with 40 water molecules (Fig. 1B), consistent with the relatively large size of $C_2O_4^{2-}$, which would require more water to achieve the same coverage as in $SO_4^{2-}(H_2O)_n$.

But what is the nature of the intense high binding energy feature in the large solvated clusters? This feature could not be accounted for by inelastic scatterings of the solute photoelectrons by the solvent for two reasons. First, this peak was too intense. The mass signals became weaker for larger solvated clusters. However, we observed that the total electron count rates, almost all due to the high binding energy peak, were in fact very strong for the large clusters. Second, we did not observe significant inelastic scatterings at 193 nm. The intense high binding energy feature must correspond to a new detachment channel, which we attribute to ionization of the solvent. The ionization potentials of water clusters should be between that of gaseous water molecules at 12.6 eV and that of liquid water at 10.06 eV (*30*). Because our solvated clusters were negatively charged, the ionization potentials of water should be lowered. In fact, we recently observed that the ionization potential of a water molecule was reduced from 12.6 eV to about 6.1 eV in the F^-H_2O complex (*31*), because of the strong Coulomb repulsion experienced by the valence electrons in H_2O from F^-. We further observed that the intensity of the solvent ionization peak increased rapidly with the solvent number. In the present study, the ionization of water could not be observed in the small clusters because of the cutoff due to the RCB (*17*). The decrease of the RCB and the enhanced ionization cross section with increasing solvent number caused the signals from ionizing the solvent to become the dominant PES feature in the large clusters of $SO_4^{2-}(H_2O)_n$ and $C_2O_4^{2-}(H_2O)_n$.

Because of the overlap between the solvent ionization feature and features due to the solute, we could not definitively identify the precise cluster size where the solvent ionization feature appeared. However,

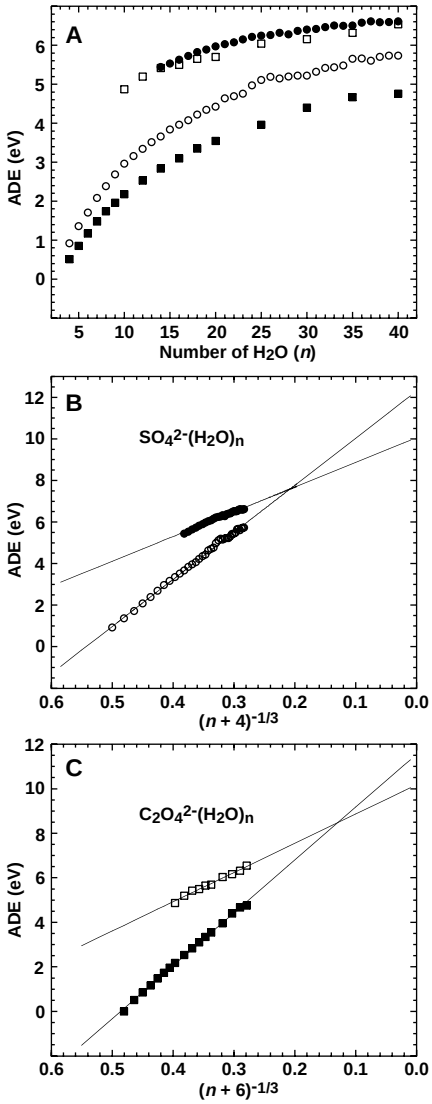

Fig. 2. (**A**) Adiabatic detachment energies (ADE) or ionization thresholds of SO_4^{2-} (○) and H_2O (●) in $SO_4^{2-}(H_2O)_n$ and $C_2O_4^{2-}$ (■) and H_2O (□) in $C_2O_4^{2-}(H_2O)_n$ as a function of solvent number (n). (**B**) ADE of SO_4^{2-} (○) and H_2O (●) in $SO_4^{2-}(H_2O)_n$ as a function of $(n + 4)^{-1/3}$ (proportional to the reciprocal of the cluster radius). (**C**) ADE of $C_2O_4^{2-}$ (■) and H_2O (□) in $C_2O_4^{2-}(H_2O)_n$ as a function of $(n + 6)^{-1/3}$ (proportional to the reciprocal of the cluster radius).

we suspected that for the $SO_4^{2-}(H_2O)_n$ system (Fig. 1A), the relative intensity change between the first two solute bands starting around $n = 12$ was due to the contribution of the water ionization feature to the second solute band. Furthermore, the closing separation between the first and second bands starting in the same size range suggested that the binding energy for the ionization of water was actually smaller than that of the second solute band. Therefore, the threshold of the second band at large n actually represented the ionization threshold of the solvent. For the $SO_4^{2-}(H_2O)_n$ system, we obtained the ionization threshold of water for $n > 13$. The spectra of $C_2O_4^{2-}$-$(H_2O)_n$ (Fig. 1B) showed that the third PES band began to dominate above $n = 10$, again indicating major contributions of solvent ionization to this band. Our estimated solvent ionization thresholds for the two systems, along with those obtained for the solutes, are plotted in Fig. 2A as a function of solvent number (*32*). We note that the solvent ionization thresholds were nearly identical in the two systems, but the detachment thresholds of SO_4^{2-} were systematically larger than that of $C_2O_4^{2-}$ for a given solvent number.

Previous theoretical considerations of ion solvation in finite clusters suggested that the ionization energies of a solvated anion should be scaled to $1/R$ linearly (*13, 33*), where R is the radius of the solvated clusters and is proportional to the solvent number as $(n + \delta)^{-1/3}$ (where δ is the equivalent solvent number for the solute and accounts for the contribution of the solute to the cluster volume). For example, in $I^-(H_2O)_n$, δ has been taken to be 2 for I^- (*7*). We estimated that δ is 4 for SO_4^{2-} and 6 for $C_2O_4^{2-}$. In Fig. 2, B and C, we plot the ionization thresholds for the solutes and solvent as a function of $(n + \delta)^{-1/3}$. The ionization thresholds for the solutes as well as that for water were indeed linearly dependent on $(n + \delta)^{-1/3}$ for both solvated systems.

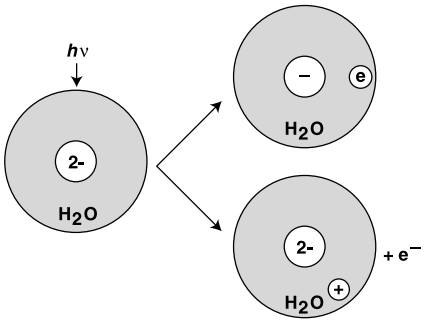

Fig. 3. Schematic illustration of the photophysical processes taking place in the water nanodroplets doped with a doubly charged anion, showing the trapping of the photoelectron from the solute (**top**) and the ionization of the solvent (**bottom**).

For infinite n, the ionization energies for water can be extrapolated to 10.05 and 10.2 eV for the $SO_4^{2-}(H_2O)_n$ and $C_2O_4^{2-}(H_2O)_n$ systems, respectively; these values are consistent with the threshold ionization energy of bulk water at 10.06 eV. This observation lent considerable credence for the assignment of the high binding energy feature to ionization of water in both solvated systems. The ionization energies of the solutes can each be extrapolated to a very large value for infinitely large clusters: 12.3 eV for $SO_4^{2-}(H_2O)_n$ and 11.5 eV for $C_2O_4^{2-}$-$(H_2O)_n$. In bulk aqueous solutions, the threshold ionization energies of SO_4^{2-} and $C_2O_4^{2-}$ were measured to be 8.65 and 7.32 eV, respectively (*30*). The discrepancies between our extrapolated values and the bulk values can be attributed to the fact that the bulk values were measured over the surface of electrolyte solutions at relatively high solute concentrations, whereas our extrapolations corresponded to a hypothetical situation in which a single solute is solvated in the center of an infinitely large water cluster (i.e., an infinitely dilute solution).

The dimensions of our largest solvated clusters were greater than 1 nm. We observed that these water nanodroplets doped with a single solute molecule began to exhibit electronic properties similar to bulk electrolyte solutions. A smooth transition from solvated molecular clusters to behaviors of electrolyte solutions was thus observed one solvent molecule at a time. The photophysical process in the large solvated clusters is schematically illustrated in Fig. 3. Although photoemission from the solute dominated in small clusters, photoelectrons from the solutes were trapped by the solvent in the large clusters, producing "solvated" electrons (instead of electron emission to vacuum), analogous to the generation of solvated electrons in bulk aqueous solutions (*34*). The ionization of the solvent, however, would produce a "hole" that could react with the solutes through charge migration or react with a neighboring water molecule to generate $OH + H_3O^+$, a process known to occur in bulk solutions (*34*). These photophysical processes taking place in the solvated clusters may be investigated using pump-probe experiments (*12, 35, 36*). Therefore, the solvated nanoclusters, in addition to being structural models, may be used as molecular analogs for the investigation of a variety of properties of aqueous electrolyte solutions.

References and Notes

1. A. Pasquarello *et al.*, *Science* **291**, 856 (2001).
2. H. Ohtaki, T. Radnai, *Chem. Rev.* **93**, 1157 (1993).
3. G. Niedner-Schatteburg, V. E. Bondybey, *Chem. Rev.* **100**, 4059 (2000).
4. E. M. Knipping *et al.*, *Science* **288**, 301 (2000).
5. D. C. Clary, D. M. Benoit, T. V. Mourik, *Acc. Chem. Res.* **33**, 441 (2000).
6. V. A. Parsegian, *Nature* **378**, 335 (1995).
7. G. Markovich, S. Pollack, R. Giniger, O. Cheshnovsky, *J. Chem. Phys.* **101**, 9344 (1994).
8. L. Perera, M. L. Berkowitz, *J. Chem. Phys.* **99**, 4222 (1993).
9. _____, *J. Chem. Phys.* **100**, 3085 (1994).
10. P. Ayotte, G. H. Weddle, M. A. Johnson, *J. Chem. Phys.* **110**, 7129 (1999).
11. O. M. Cabarcos, C. J. Weinheimer, J. Lisy, S. S. Xantheas, *J. Chem. Phys.* **110**, 5 (1999).
12. L. Lehr, M. T. Zanni, C. Frischkorn, R. Weinkauf, D. M. Neumark, *Science* **284**, 635 (1999).
13. I. Rips, J. Jortner, *J. Chem. Phys.* **97**, 536 (1992).
14. D. A. Yarne, M. E. Tuckerman, M. L. Klein, *Chem. Phys.* **258**, 163 (2000).
15. M. R. Waterland, D. Stockwell, A. M. Kelley, *J. Chem. Phys.* **114**, 6249 (2001).
16. J. M. Weber, J. A. Kelley, S. B. Nielsen, P. Ayotte, M. A. Johnson, *Science* **287**, 2461 (2000).
17. L. S. Wang, X. B. Wang, *J. Phys. Chem. A* **104**, 1978 (2000).
18. A. Blades, P. Kebarle, *J. Am. Chem. Soc.* **116**, 10761 (1994).
19. E. V. Stefanovich, A. I. Boldyrev, T. N. Truong, J. Simons, *J. Phys. Chem. B* **102**, 4205 (1998).
20. W. R. Cannon, B. M. Pettitt, J. A. McCammon, *J. Phys. Chem.* **98**, 6225 (1994).
21. H. Siegbahn, *J. Phys. Chem.* **89**, 897 (1985).
22. R. Bohm, H. Morgner, J. Oberbrodhage, M. Wulf, *Surf. Sci.* **317**, 407 (1994).
23. M. Faubel, B. Steiner, J. P. Toennies, *J. Chem. Phys.* **106**, 9013 (1997).
24. J. V. Coe *et al.*, *J. Chem. Phys.* **92**, 3980 (1990).
25. J. V. Coe *et al.*, *J. Chem. Phys.* **107**, 6023 (1997).
26. X. B. Wang, J. B. Nicholas, L. S. Wang, *J. Chem. Phys.* **113**, 10837 (2000).
27. L. S. Wang, C. F. Ding, X. B. Wang, S. E. Barlow, *Rev. Sci. Instrum.* **70**, 1957 (1999).
28. X. Yang, X.-B. Wang, J. B. Nicholas, L.-S. Wang, unpublished data.
29. J. Dietter, H. Morgner, *Chem. Phys.* **220**, 261 (1997).
30. P. Delahay, *Acc. Chem. Res.* **15**, 40 (1982).
31. X. Yang, X. B. Wang, L. S. Wang, *J. Chem. Phys.* **115**, 2889 (2001).
32. Although the solvent PES feature was most likely cut off by the RCB, the solvent ionization threshold could still be determined. The thresholds were estimated by drawing a straight line at the leading edge of the relevant photodetachment band and adding the instrumental resolution to the intercept with the binding energy axis. The uncertainties were ±0.1 eV for well-defined photoelectron bands and were larger (±0.15 eV) for weaker features in the large solvated systems and the ionization thresholds of water in $C_2O_4^{2-}(H_2O)_n$ because of the overlap with the solute features (Fig. 1B).
33. R. N. Barnett, U. Landman, C. L. Cleveland, J. Jortner, *Chem. Phys. Lett.* **145**, 382 (1988).
34. R. A. Crowell, D. M. Bartels, *J. Phys. Chem.* **100**, 17940 (1996).
35. B. J. Schwartz, P. J. Rossky, *J. Chem. Phys.* **101**, 6917 (1994).
36. C. Silva, P. K. Walhout, K. Yokoyama, P. F. Barbara, *Phys. Rev. Lett.* **80**, 1086 (1998).
37. For supplemental material, see *Science* Online (www.sciencemag.org/cgi/content/full/294/5545/1322/DC1).

38. We thank A. I. Boldyrev and J. P. Cowin for valuable discussions. Supported by the U.S. Department of Energy (DOE), Office of Basic Energy Sciences, Chemical Science Division. The work was performed at the W. R. Wiley Environmental Molecular Sciences Laboratory, a national scientific user facility sponsored by DOE's Office of Biological and Environmental Research and located at Pacific Northwest National Laboratory, operated for DOE by Battelle.

31 July 2001; accepted 21 September 2001